Designing Optimal Pulse-Shapers for Ultra-Wideband Radios

Xiliang Luo, Liuqing Yang, and Georgios B. Giannakis

Abstract: **Ultra-wideband (UWB) technology is gaining increasing interest for its potential application to short-range indoor wireless communications. Utilizing ultra-short pulses, UWB baseband transmissions enable rich multipath diversity, and can be demodulated with low complexity receivers. Compliance with the FCC spectral mask, and interference avoidance to, and from, co-existing narrow-band services, calls for judicious design of UWB pulse shapers. This paper introduces pulse shaper designs for UWB radios, which optimally utilize the bandwidth and power allowed by the FCC spectral mask. The resulting baseband UWB systems can be either single-band, or, multi-band. More important, the novel pulse shapers can support dynamic avoidance of narrow-band interference, as well as efficient implementation of fast frequency hopping, without invoking analog carriers.**

Index Terms: **Ultra-wideband (UWB), pulse shaper, FCC spectral mask, multi-band, time hopping (TH), frequency hopping (FH).**

I. INTRODUCTION

Ultra-wideband (UWB) radios (a.k.a. Impulse Radios) are gaining increasing interest from industry, government, and academia, for their potential especially in the area of short-range indoor wireless communications [1]. Utilizing pulses of duration in the order of a nanosecond, UWB transmissions enable rich multipath diversity. In baseband operation, UWB transceivers are also carrier-free, and can thus be implemented with low complexity.

Occupying extremely broad bandwidth, UWB radios inevitably have to overlay existing narrow-band RF services, such as the global positioning system (GPS), federal aviation systems (FAS), and wireless local area networks (WLAN). To regulate co-existence, the Federal Communications Commission (FCC) has released a spectral mask in its "First UWB Report and Order (R&O)" [2], that limits the equivalent isotropic radiated power (EIRP) spectrum density with which UWB radios are allowed to transmit. In order to realize the attractive features of UWB radios under this FCC regulation, the following challenges have to be addressed:

i) Operating below the noise floor, UWB radios must emit at low-power. But as any other communication system, the performance of a UWB system heavily relies on the received signal-to-noise-ratio (SNR), which is proportional to the transmit power. Maximization of the latter, however, can be achieved only if the spectral shape of the FCC mask is exploited in a power-efficient manner.

ii) To avoid interference to (and from) co-existing narrow-band systems, their corresponding frequency bands must be avoided. Since the nature and number of co-existing services may change depending on the band used, the avoidance mechanism should also allow for sufficient flexibility.

iii) Traditionally, UWB multiple access is achieved by employing time hopping (TH) codes [3], [4]. User capacity of UWB radios can be further improved by partitioning the ultra-wide bandwidth into sub-bands, allowing users to hop among these sub-bands according to user-specific hopping patterns. Since hopping takes place over sub-bands centered around different frequencies, similar to narrow-band systems, frequency hopping (FH) can also enhance system capacity, and reinforce the low probability of interception/detection (LPI/LPD) of UWB radios.

All these requirements heavily rely on a basic transmitter module – the pulse shaper. Unfortunately, the widely adopted Gaussian monocycle is not flexible enough to meet these challenges [5]. To design pulse shapers with desirable spectral properties, two approaches can be employed: Carrier-modulation and/or baseband analog/digital filtering of the baseband pulse shaper. The former relies on local oscillators at the UWB transmitter and receiver, which being prone to mismatch give rise to carrier frequency offset/jitter (CFO/CFJ). In multi-band UWB systems with FH, multiple CFO/CFJ's emerge with this approach. Although passing the (Gaussian) pulse through a baseband analog filter can re-shape the pulse without introducing CFO/CFJ, it is well known that analog filters are not as flexible when compared to digital filters, which are accurate, highly linear, and perfectly repeatable [6].

To this end, this paper introduces optimal pulse shapers for UWB using the "workhorse" of digital filter design methods, namely the Parks-McClellan algorithm [6, Chaper 7]. The resulting pulse shapers exploit the FCC spectral mask optimally, and offer flexibility for (dynamic) avoidance of narrow-band interference (NBI). Equally important, multi-band UWB with fast FH can also be implemented digitally using the novel baseband pulse shapers.

Pulse shapers respecting the FCC spectral mask were proposed recently in [7] and [8]. Targeting multiple orthogonal pulses that are FCC mask compliant, the resulting pulses in digital form correspond to the dominant eigenvectors of a matrix,

Manuscript received August 5, 2003.

The authors are with the Department of Electrical and Computer Engineering, University of Minnesota, 200 Union Street SE, Minneapolis, MN 55455, USA. Tel/fax: (612)626-7781/625-4583, email: {xlluo, lqyang, georgios}@ece.umn.edu.

This work was supported by the NSF grant No. EIA-0324864, and collaborative participation in the Communications and Networks Consortium sponsored by the U. S. Army Research Laboratory under the Collaborative Technology Alliance Program, Cooperative Agreement DAAD19-01-2-0011. The U.S. Government is authorized to reproduce and distribute reprints for Government purposes notwithstanding any copyright notation thereon. The material in this paper was presented in part at the *IEEE Conf. on Ultra-Wideband Systems and Technologies*, Reston, VA, Nov. 2003.

which is constructed by sampling the FCC mask [7]. Different from these pulse shapers, our designs not only offer optimality in *meeting* the FCC mask, but also *optimally exploit* the allowable bandwidth and power. Moreover, converting the digital designs in [7] into analog form entails digital-to-analog (D/A) operations at 64GHz rate; whereas our designs can be implemented without requiring expensive ADC circuitry and without modifying the analog components of existing UWB transmitters [5].

The rest of the paper is organized as follows. The transmit spectrum and its relation to the underlying UWB pulse shaper is given in Section II. The optimal pulse design methodology is developed in Section III, while Section IV analyzes the impact of these designs in mitigating NBI. The effects of clock jitter and comparisons with the analog carrier-modulated UWB systems in the presence of CFO/CFJ, are analyzed in Section V. In Sections VI and VII, design examples and simulated comparisons are presented. Finally, concluding remarks are offered in Section VIII.

II. TRANSMIT SPECTRUM AND PULSE SHAPER

A typical modulation in UWB radios is binary pulse position modulation (PPM), in conjunction with time hopping (TH) codes that are used to enable multiple access (MA) and smooth the transmit-spectra [3]. With $p(t)$ denoting the pulse shaper with $\mathcal{E}_p := \int p^2(t)dt$, the emitted waveform from a single UWB transmitter is

$$u(t) = \sum_k \sqrt{\frac{\mathcal{E}}{\mathcal{E}_p}}\, p(t - kT_f - c_kT_c - s(\lfloor k/N_f \rfloor)\,\Delta), \qquad (1)$$

where $\mathcal{E}$ is the transmitted energy per pulse, T_f is the frame duration consisting of N_c chips, $c_k \in [0, N_c - 1]$ is the N_f-periodic TH sequence, T_c is the chip period, $s(n)$ represents the information symbol, and Δ is the PPM modulation index. With k indexing frames in (1), each information symbol is transmitted over N_f frames, which explains the floor operation $\lfloor k/N_f \rfloor$, and implies that the effective symbol duration is $T_s := N_fT_f$. To implement TH, each frame is divided into N_c chips, each of duration T_c, i.e., $T_f = N_cT_c$. Upon defining the symbol level pulse shaper as

$$p_s(t) = \sum_{k=0}^{N_f-1} \frac{1}{\sqrt{\mathcal{E}_p}} p(t - kT_f - c_kT_c), \qquad (2)$$

the transmitted signal can be rewritten as $u(t) = \sum_n \sqrt{\mathcal{E}} p_s(t - nT_s - s(n)\Delta)$. The power spectrum density (PSD) of the latter can be calculated as in [9, Chapter 4]

$$\Phi_{uu}(f) = \mathcal{E}\frac{1}{T_s}|P_s(f)|^2 \times \left[\frac{1-\cos(2\pi\Delta f)}{2} + \frac{1+\cos(2\pi\Delta f)}{2T_s}\sum_{k=-\infty}^{+\infty}\delta(f - \frac{k}{T_s})\right], \qquad (3)$$

where $P_s(f)$ is the Fourier Transform (FT) of $p_s(t)$, whose nonzero frequency support is determined by the pulse shaper $p(t)$, and its shape depends on the specific TH code c_k [c.f. (2)]. Specifically, based on (2) and (3), we can easily verify that

$$\Phi_{uu}(f) = \frac{\mathcal{E}}{\mathcal{E}_p}\frac{1}{T_f}|P(f)|^2\rho_1(f), \qquad (4)$$

where

$$\rho_1(f) := \frac{\left|\sum_{k=0}^{N_f-1} e^{-j2\pi fkT_f}e^{-j2\pi fc_kT_c}\right|^2}{N_f} \times \left[\frac{1-\cos(2\pi\Delta f)}{2} + \frac{1+\cos(2\pi\Delta f)}{2T_s}\sum_{k=-\infty}^{+\infty}\delta(f-\frac{k}{T_s})\right].$$

Equation (4) is a special case of [10], where a general PSD expression allowing for (even long) deterministic TH codes is derived. When c_k in (1) is integer-valued independent and uniformly distributed over $[0, N_c - 1]$ as in [11], the PSD is still given by (4) but with $\rho_1(f)$ replaced by

$$\rho_2(f) = 1 - \frac{1+\cos(2\pi\Delta f)}{2}\left|\frac{\sin(\pi fT_cN_c)}{\sin(\pi fT_c)}\right|^2\frac{1}{{N_c}^2} + \frac{1+\cos(2\pi\Delta f)}{2}\frac{1}{T_f}\sum_{k=-\infty}^{+\infty}\delta(f-\frac{k}{T_c}). \qquad (5)$$

Although $\rho_1(f)$ and $\rho_2(f)$ contain spectral spikes, the severity of interference from UWB transmissions to co-existing systems depends on the average power, which entails integration of the PSD over the band (say $[f_1, f_2]$) that the victim system(s) operates in. For this reason, integrating $\rho_1(f)$ and $\rho_2(f)$ yields approximately:

$$\int_{f_1}^{f_2}\rho_1(f)df \simeq \int_{f_1}^{f_2}\rho_2(f)df \simeq \int_{f_1}^{f_2}1df = f_2 - f_1, \qquad (6)$$

where f_1, f_2 are two frequencies satisfying $f_2 - f_1 > 1/T_f$. Substituting (6) into (4) implies that we can approximate the EIRP spectrum of a single UWB transmitter as [c.f. (1)]

$$\Phi_{EIRP}(f) \cong \frac{\mathcal{E}}{\mathcal{E}_p}\frac{|P(f)|^2}{T_f}. \qquad (7)$$

FCC requires that EIRP spectra emitted by indoor UWB radios must adhere to the spectral mask depicted in Fig. 1(a) [2]. In order to satisfy the FCC power emission limit, we need to keep $\Phi_{EIRP}(f)$ below the prescribed spectral mask. Evidently, this can be achieved for any $p(t)$ by confining $\mathcal{E}$ to sufficiently low values. But recall that symbol detection performance depends on the SNR, which is proportional to $\mathcal{E}$. Therefore, it is desirable to design pulse shapers that allow for efficient exploitation of the FCC mask.

Before introducing our pulse shaper designs, let us first consider the Gaussian pulse, which has been widely adopted by UWB radar and communication systems [12]. With the Gaussian pulse as input, the UWB antenna acts as a differentiator [13] to produce naturally at its output the first derivative of the Gaussian pulse, which is known as the Gaussian monocycle [5]. Since the transmit spectrum depends on the pulse shape at the

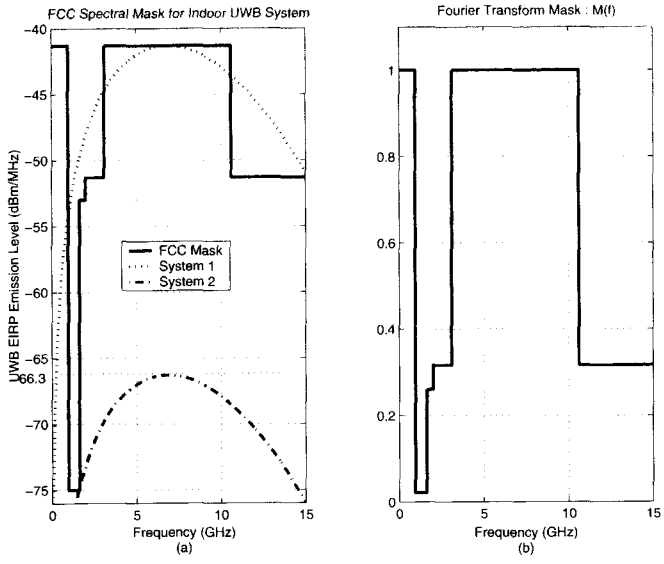

Fig. 1. (a) Solid: FCC spectral mask for indoor UWB system. Dotted: System 1, whose PSD violates the spectral mask over 1-3GHz. Dash-dotted: System 2, whose PSD satisfies the spectral mask. (b) Fourier Transform mask.

output of the antenna, we will henceforth consider the pulse shaper incorporating the aggregate effects of the on-chip pulse in cascade with the transmit antenna. The Gaussian monocycle can be expressed as

$$g(t) = 2\sqrt{e}A\frac{t}{\tau_g}e^{-2(\frac{t}{\tau_g})^2}, \tag{8}$$

where τ_g is the time duration between its minimum and maximum values and A represents its peak amplitude. The pulse duration is approximately $T_g = 4\tau_g$. Accordingly, the FT of $g(t)$ is

$$G(f) = \frac{1}{2}\sqrt{\frac{2e}{\pi}}\frac{Af}{f_g^2}e^{-\frac{1}{2}(\frac{f}{f_g})^2}, \tag{9}$$

where $f_g := 1/(\pi\tau_g)$ is the frequency where $|G(f)|$ is maximum. Letting $p(t) = g(t)$ in (1), the transmit EIRP spectrum is depicted in Fig. 1(a) for two values of transmit-power: a prohibitively high power (System 1), and a sufficiently low power (System 2). Trying to maximize transmission power, System 1 violates the FCC spectrum mask; whereas trying to respect the FCC mask at the forbidden bands, System 2 does not exploit the FCC mask in a power efficient manner. Consequently, the Gaussian monocycle does not lead to optimal utilization of the spectrum assigned by FCC. Moreover, utilization of the entire bandwidth entails circuits and processors with enormous frequency response. The payback, however, may not be as handsome, due to the increasingly lossy nature of high frequency bands. Therefore, it is sometimes desirable to use only a fraction of the entire bandwidth, which also facilitates NBI suppression. Furthermore, partitioning the entire bandwidth, and letting each user utilize only a fraction of it, enables multiple access via frequency hopping (FH). Although readily implementable [14], [15], the Gaussian monocycle does not provide us with such capability and flexibility, unless it is employed after some processing. These considerations give rise to the following question:

Using the Gaussian monocycle $g(t)$, that constitutes the antenna's physical response, as the elementary building block, can we optimally design $p(t)$ with desirable spectral characteristics?

In the next section, we will introduce our methodology for designing optimum or sub-optimum pulse shapers based on the basic Gaussian monocycle.

III. OPTIMAL PULSE DESIGN

As we discussed in Section II, the transmit EIRP spectrum is directly related to $P(f)$. In order to utilize the FCC spectral mask efficiently, the magnitude $|P(f)|$ needs to closely approximate the shape of the spectral mask, which translates to a desired magnitude profile $P_d(f)$. We will show later that $P_d(f)$ can be chosen to satisfy *any* desirable specifications, which explains why we did not limit ourselves to desired pulses with $P_d^2(f)$ equal to the FCC spectral mask. The problem statement is:

Given i) the Gaussian monocycle $g(t)$ whose shape is uniquely determined by τ_g or, equivalently, f_g [c.f. (8), (9)]*; and ii) the desired FT magnitude $P_d(f)$, we want to design $p(t)$ so that $|P(f)|$ approximates $P_d(f)$ in some meaningful sense of optimality.*

Normalizing the square root of the FCC spectral mask to a Fourier Transform mask $\mathcal{M}(f)$, with $\max\{\mathcal{M}(f)\} = 1$ (see Fig. 1(b)), it follows that $P_d(f)$ is upper bounded by $\mathcal{M}(f)$. Our key idea is to design $p(t)$ as:

$$p(t) = \sum_{n=0}^{M-1} w[n]g(t - nT_0), \tag{10}$$

where $w[n]$ are tap coefficients with spacing T_0. As we will discuss later, the choice of T_0 affects $w[n]$, and thus the feasibility, optimality, and complexity of the overall design. It can be easily verified that the FT of $p(t)$ is given by [c.f. 10]:

$$P(f) = W(e^{j2\pi fT_0})G(f), \tag{11}$$

where $W(e^{j2\pi fT_0}) := \sum_{n=0}^{M-1} w[n]e^{-j2\pi fT_0 n}$, is periodic with period $(1/T_0)$Hz. Furthermore, with $\{w[n]\}_{n=0}^{M-1}$ being real, $|W(e^{j2\pi fT_0})|$ is symmetric around $f = 0$. Consequently, we can uniquely control $|P(f)|$ only over the band $[0, 1/(2T_0)]$, since outside this band $W(e^{j2\pi fT_0})$ is replicated periodically. This implies that depending on the prescribed band of interest, T_0 needs to be selected accordingly (we will see specific cases later).

Having selected T_0, our $p(t)$ design problem is equivalent to the following one:

Find M tap coefficients: $w[0], \cdots, w[M-1]$, so that the function $|W(e^{j2\pi fT_0})|$ satisfies:

$$|W(e^{j2\pi fT_0})| : \begin{cases} \approx \frac{P_d(f)}{|G(f)|}, & f \in [0, \frac{1}{2T_0}] \\ < \frac{\mathcal{M}(f)}{|G(f)|}, & f \in [\frac{1}{2T_0}, +\infty]. \end{cases} \tag{12}$$

Notice that apart from compliance to the normalized FCC mask, we attach no strings on our filter taps $\{w[n]\}_{n=0}^{M-1}$ outside the controllable band of interest. This will allow flexibility in selecting T_0 and will also lead to a parsimonious design

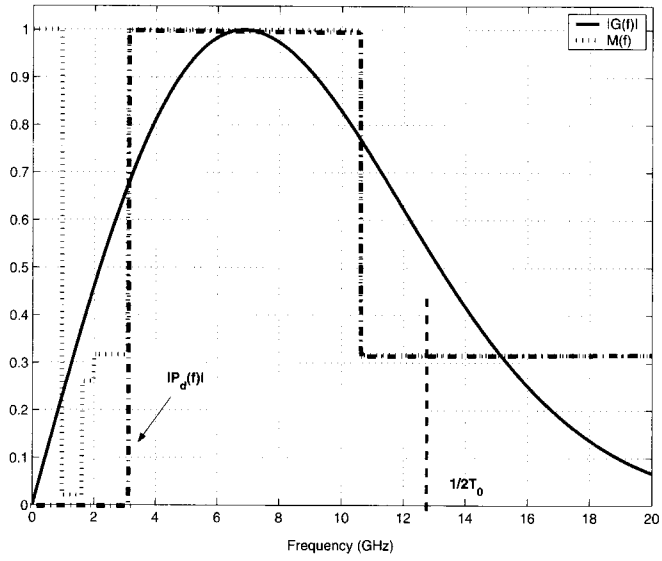

Fig. 2. FT of Gaussian monocycle with $f_g = 6.85$GHz vs. Fourier Transform mask $M(f)$.

with small M, and thus low implementation complexity. Furthermore, if f_g in (9) is also specified, the pulse shaper design problem boils down to a Finite Impulse Response (FIR) filter design problem:

Design an M-tap FIR filter with coefficients: $w[0], \cdots, w[M-1]$, *so that its Discrete Time Fourier Transform (DTFT) magnitude* $|W(e^{j2\pi F})|$ *approximates the function* $D(F/T_0)$, $F \in [0, 0.5]$, *where* $D(f) := P_d(f)/|G(f)|, f \in [0, \frac{1}{2T_0}]$.

Among various FIR filter design methods, the IDFT one is the easiest to implement, but does not offer flexibility in approximating $D(F/T_0)$. Furthermore, aiming at low complexity implementation, we wish to minimize the number of taps M, which in turn will minimize the time duration of the resultant pulse shaper for a given T_0, since $T_p = T_g + (M-1)T_0$. These considerations motivate us to adopt the Parks-McClellan algorithm [6, Chapter 7], which leads to pulse shaper designs that are optimal in the sense that they minimize the maximum approximation error over the frequency band of interest. For simplicity, we choose linear phase filter approximants with symmetric taps, i.e., $w[n] = w[2L-n]$ for $n = 0, \cdots, 2L$. Instead of $M = 2L+1$ coefficients, it then suffices to design $L+1$ taps $\{w[n]\}_{n=0}^{L}$, because upon defining $w_L[n] = w[n+L]$, we have $W_L(e^{j2\pi F}) = \sum_{n=-L}^{L} w_L[n]e^{-j2\pi Fn} = w_L[0] + \sum_{n=1}^{L} 2w_L[n]\cos(2\pi Fn)$, and $|W_L(e^{j2\pi F})| = |W(e^{j2\pi F})|$. The pulse design problem now is equivalent to:

Let $\mathcal{F}$ *represent a union of prescribed disjoint intervals in* $[0, 0.5]$, *so that* $D(F/T_0)$ *is continuous in each interval. Choose taps* $\{w_L[n]\}_{n=0}^{L}$ *according to the optimality criterion :*

$$\min_{\{w_L[n]\}_{n=0}^{L}} \left\{ \max_{F\in\mathcal{F}} |e(F)| \right\}, \tag{13}$$

where $e(F) := \lambda(F)[D(F/T_0) - W_L(e^{j2\pi F})]$ *is the error function, and* $\lambda(F)$ *denotes a positive weight function.*

This problem turns out to be a Chebyshev approximation problem with desired function $D(F/T_0)$, and can be solved numerically based on the "Alternation Theorem" in polynomial approximation theory [16].

A. Single-Band UWB

In order to utilize the entire bandwidth from 3.1GHz to 10.6GHz, the $P_d(f)$ must be as in Fig. 2, where we have intentionally set $P_d(f) = 0$, $\forall f < 3.1$GHz to avoid interference to GPS. Recall also that the tap spacing T_0 should be chosen depending on the band region in which we want to control the pulse shaper design. We will distinguish between the following two cases:

A.1 Full Band Control

Since $W_L(e^{j2\pi fT_0})$ is symmetric around $1/(2T_0)$ and repeats every $(1/T_0)$GHz, to gain full control over the entire band $[3.1, 10.6]$GHz, it is necessary for T_0 to obey $1/(2T_0) > 10.6$GHz. Recall now that our linear phase filter $W_L(e^{j2\pi fT_0})$ must satisfy [c.f. (12)]

$$|W_L(e^{j2\pi fT_0})| : \begin{cases} \approx D(f) = \frac{P_d(f)}{|G(f)|} & f \in [0, \frac{1}{2T_0}] \\ < \frac{\mathcal{M}(f)}{|G(f)|} & f > \frac{1}{2T_0}, \end{cases} \tag{14}$$

where $\mathcal{M}(f)$ is the Fourier transform mask. Under the constraint $1/(2T_0) > 10.6$GHz, we will select T_0 to fulfill (14) for $f > 1/(2T_0)$; i.e., to obey $|W_L(e^{j2\pi fT_0})G(f)| < \mathcal{M}(f)$ for $f > 1/(2T_0)$. Because $|G(f)|$ decreases monotonically for $f > 1/(2T_0)$, it suffices to enforce this last inequality for a fixed point f_0, where $|W_L(e^{j2\pi fT_0})|$ achieves its maximum, since then $|W_L(e^{j2\pi fT_0})G(f)| < |W_L(e^{j2\pi f_0T_0})G(f_0)|, \forall f > f_0$, by the monotonicity of $|G(f)|$ and the periodicity of $|W_L(e^{j2\pi fT_0})|$. Based on these considerations, we choose this point to be $f_0 = 1/T_0 - 10.6$GHz.

At this point, we have $|G(f_0)| = |G(1/T_0 - 10.6\text{GHz})|$, and $|W_L(e^{j2\pi f_0T_0})| = |W_L(e^{j2\pi 10.6T_0})|$ by the periodicity. As in Fig. 2, we have $P_d(10.6) = 1$, which implies that $|W_L(e^{j2\pi 10.6T_0})| \simeq P_d(10.6)/|G(10.6)| = 1/|G(10.6)|$. Therefore, selecting T_0 to satisfy (14) for $f_0 = 1/T_0 - 10.6$GHz amounts to choosing T_0 so that

$$\frac{\left|G\left(\frac{1}{T_0} - 10.6\right)\right|}{|G(10.6)|} < \mathcal{M}\left(\frac{1}{T_0} - 10.6\right). \tag{15}$$

But since the $\mathcal{M}(f)$ prescribed by FCC is constant when $f > 10.6$GHz, and $G(f)$ is given by (9), solving for the set of T_0's satisfying (15) is straightforward.

To ease implementation of (10), we will always select the smallest possible T_0. The latter certainly depends also on the Gaussian monocycle parameter f_g. For instance, when $f_g = 6.85$GHz, which is the center of the allocated UWB band, we can choose $T_0 = 35.7$ps in order to satisfy (15). With T_0 specified, $D(F/T_0)$ is continuous within three intervals: $\mathcal{I}_1 = (0, 3.1T_0), \mathcal{I}_2 = (3.1T_0, 10.6T_0)$, and $\mathcal{I}_3 = (10.6T_0, 0.5)$. We choose the set $\mathcal{F}$ in (13) to be $\mathcal{F} = \mathcal{F}_1 \bigcup \mathcal{F}_2 \bigcup \mathcal{F}_3$, where $\mathcal{F}_1 \subset \mathcal{I}_1$, $\mathcal{F}_2 \subset \mathcal{I}_2$, and $\mathcal{F}_3 \subset \mathcal{I}_3$[1]. With an appropriately selected weight function $\lambda(F)$ in (13), the optimum tap coefficients $\{w[n]\}_{n=0}^{M-1}$ can be found and the pulse shaper can be subsequently obtained via (10).

[1]The transition interval should be appropriately selected, otherwise, the designed filter length will be large when small approximation error is desired.

A.2 Exploiting Symmetry to Halve the Clock Rate

In the preceding section, we have seen that with $f_g = 6.85$GHz, a clock period $T_0 = 35.7$ps is required to design the optimal pulse shaper for a single-band UWB system. Because we have full control over the entire bandwidth of $0 - 10.6$GHz, pulse shapers so designed can closely approximate the FCC mask throughout the bandwidth. However, this short clock period may impose implementation difficulty. We will show next that sub-optimum alternatives are possible for single-band UWB with larger T_0 (and thus smaller clock periods). With $f_g = 6.85$GHz, we can take advantage of the symmetry of $D(f)$ in (14) (see Fig. 2) and control $P(f)$ only over the lower half of the entire band, i.e., over the interval $[0, 6.85]$GHz, by doubling the T_0 value. Specifically, we can select $1/(2T_0) = 6.85$GHz, which corresponds to $T_0 = 73$ps. This choice does not guarantee that the FCC mask is well approximated over the entire bandwidth, unless $D(f)$ is perfectly symmetric around 6.85GHz. To approximate the normalized mask $\mathcal{M}(f)$, we look for a symmetric desired function $D_{sym}(f)$ so that:

$$D_{sym}(f) = \begin{cases} 0, & f \in [0, 3.1] \\ \min\{D(f), D(13.7 - f)\}, & f \in [3.1, 6.85], \end{cases}$$

where $D(f)$ is the desired function in (14) and $D_{sym}(F/T_0)$ is continuous in the intervals $\mathcal{I}_1 = [0, 3.1T_0]$, and $\mathcal{I}_2 = [3.1T_0, 0.5]$. We then choose the set $\mathcal{F}$ in (13) to be $\mathcal{F} = \mathcal{F}_1 \bigcup \mathcal{F}_2$, where $\mathcal{F}_1 \subset \mathcal{I}_1$, and $\mathcal{F}_2 \subset \mathcal{I}_2$. With the weight function $\lambda(F)$ being chosen appropriately, the pulse shaper can be readily designed.

B. Multi-Band UWB

As we mentioned in the Introduction, partitioning the ultra-wide bandwidth into sub-bands facilitates FH, which is important for enhancing user capacity and LPI/LPD. On the other hand, it is desirable to avoid adjacent channel interference in multi-band UWB systems by confining the spectrum of each channel within its prescribed band, while utilizing the FCC spectral mask in a power efficient manner.

Similar to the single-band pulse design, the tap spacing T_0, and thus the clock period can be selected, depending on whether full-band ($3.1 - 10.6$GHz) or half-band ($3.1 - 6.85$GHz) control is required. With full-band control, the desired functions $\{D_i(f)\}_{i=0}^{N-1}$, each corresponding to one of the total N sub-bands, are

$$D_i(f) = \begin{cases} 0, & f \in [0, 3.1 + i\frac{7.5}{N}]\text{GHz} \\ \frac{P_d(f)}{|G(f)|}, & f \in [3.1 + i\frac{7.5}{N}, 3.1 + (i+1)\frac{7.5}{N}]\text{GHz} \\ 0, & f \in [3.1 + (i+1)\frac{7.5}{N}, \frac{1}{2T_0}]\text{GHz}, \end{cases} \quad (16)$$

where $P_d(f)$ is the desired magnitude described in Section III-A and depicted in Fig. 2. Based on (16), pulse shapers can be designed for multi-band UWB by appropriately choosing $\lambda(F)$ and $\mathcal{F}$.

It is worth mentioning that with the same number of sub-bands N, full-band control results in N FH slots, whereas half-band control only results in $N/2$ FH slots. Clearly, on top of this optimality-complexity tradeoff, there is also a user capacity-complexity tradeoff.

Remarks: In addition to the widely-adopted Gaussian monocycle $g(t)$, any other readily available analog pulse shaper can be used as elementary building block in (10). This is because our objective functions $D(f)$ are normalized with respect to the FT of the elementary analog pulse shaper, namely $G(f)$ for the Gaussian monocycle. Furthermore, as we mentioned before, it is sometimes desirable to use only a fraction of the entire bandwidth in order to avoid NBI, or the highly-lossy high-frequency bands. In such cases, parameters T_0, and $\{w[n]\}_{n=0}^{M-1}$ can be flexibly adjusted to meet desirable spectral specifications.

IV. NARROW-BAND INTERFERENCE ISSUES

To minimize interference to and from co-existing services, our pulse shapers can be designed to impose minimum energy leakage to a prescribed band. This minimizes interference from narrow-band systems to UWB radios and vice versa. In fact, we will quantify next the impact our pulse shaper designs have on the bit error rate (BER).

Proposition 1: In a single-user UWB link over an additive white Gaussian noise (AWGN) plus NBI channel, with binary PPM and TH as in (1), the average BER with a correlation receiver is:

$$P_e = Q\left(\sqrt{\frac{N_f \mathcal{E}}{N_0(1 + \alpha\frac{J_0}{N_0})}}\right), \quad (17)$$

where $N_0/2$ is the AWGN variance, $J_0/2$ is the PSD of the NBI over the frequency band $[f_L, f_U]$, and $\alpha := \int_{f_L}^{f_U} |H(f)|^2 df / N_f$, with $H(f)$ being the FT of $h(t) := p_s(-t) - p_s(-t - \Delta)$ [c.f. (2)]

$$H(f) = (1 - e^{j2\pi f\Delta}) \left[\sum_{k=0}^{N_f - 1} e^{j2\pi k f T_f} e^{j2\pi c_k f T_c}\right] \frac{P^*(f)}{\sqrt{\mathcal{E}_p}}. \quad (18)$$

Proof: The received signal over one symbol interval $[nT_s, (n+1)T_s]$ is [c.f. (1)]: $r(t) = \sqrt{\mathcal{E}} p_s(t - nT_s - s(n)\Delta) + n(t) + i(t)$, where $n(t)$ is the AWGN with variance $N_0/2$, and $i(t)$ is the NBI with PSD given by:

$$\Phi_{ii}(f) = \begin{cases} \frac{J_0}{2}, & |f| \in [f_L, f_U] \\ 0, & \text{otherwise}, \end{cases} \quad (19)$$

where f_L and f_U are the lower and upper bounds of its spectral support. With PPM, a correlation receiver uses the template $v(t) = p_s(t - nT_s) - p_s(t - nT_s - \Delta)$. By selecting $\Delta \geq T_p$, the decision statistic for the n^{th} transmitted information symbol is:

$$\begin{aligned} r_n &= \int_{nT_s}^{(n+1)T_s} r(t)v(t)dt \\ &= \begin{cases} N_f\sqrt{\mathcal{E}} + \nu_n + \eta_n, & \text{if } s(n) = 0 \\ -N_f\sqrt{\mathcal{E}} + \nu_n + \eta_n, & \text{if } s(n) = 1, \end{cases} \end{aligned} \quad (20)$$

where

$$\nu_n := \int_{nTs}^{(n+1)T_s} n(t)v(t)dt,$$

$$\eta_n := \int_{nTs}^{(n+1)T_s} i(t)v(t)dt.$$

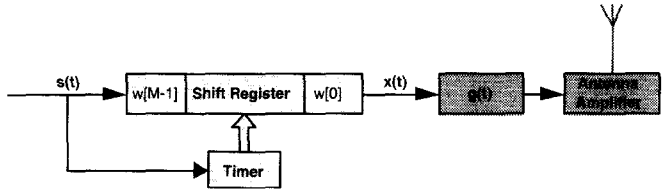

Fig. 3. Transmitter structure for single-band UWB with TH and binary PPM.

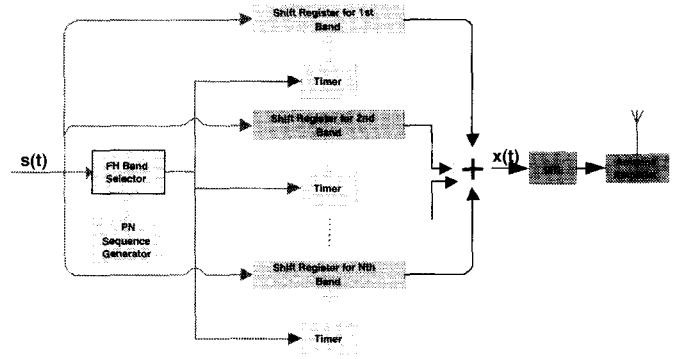

Fig. 4. Transmitter structure for multi-band UWB with fast FH and binary PPM.

It can be easily verified that ν_n is zero mean Gaussian with variance $N_f N_0$. Modelling $i(t)$ as a Gaussian random process, η_n will also be Gaussian. To derive an expression for its variance, consider $\eta(t) = \int_{-\infty}^{+\infty} i(\tau)(p_s(\tau - t) - p_s(\tau - t - \Delta))d\tau$ as the output of a linear time-invariant (LTI) system with impulse response $h(t) = p_s(-t) - p_s(-t - \Delta)$, and input $i(t)$. We find that $\eta(t)$ is Gaussian, with PSD given by $\Phi_{\eta\eta}(f) = |H(f)|^2 \Phi_{ii}(f)$, where $H(f)$ is given by (18). With $\eta_n := \eta(t)|_{t=nT_s}$, we find that $\text{var}(\eta_n) = J_0 \int_{f_L}^{f_U} |H(f)|^2 df$. Defining $\alpha := \int_{f_L}^{f_U} |H(f)|^2 df / \int_0^{+\infty} |H(f)|^2 df$, and noticing that $\int_0^{+\infty} |H(f)|^2 df = N_f$, we have that $\text{var}(\eta_n) = \alpha N_f J_0$. As a result, the average BER is given by (17). □

From Proposition 1, it is clear that the parameter α affects the BER performance by altering the effective SNR. And α is merely determined by the pulse shaper $p(t)$. With our pulse design algorithm, we can easily shape our pulse to have minimum energy over the NBI band $[f_L, f_U]$, and thus reduce BER. In Section III, we intentionally set $P_d(f) = 0$ over $[0, 3.1]$GHz to minimize the value of α, so as to mitigate the NBI within this band.

In the presence of multipath effects, NBI can be mitigated similarly by designing pulse shapers with smaller α values. This is possible because even in the presence of multipath, the variance of η_n is reduced in exactly the same way as for AWGN channels. We will also verify this by simulations when comparing the BER performance in the presence of multipath in Section VII.

V. IMPLEMENTATION ISSUES

Our pulse shapers designed as in (10) can be implemented using currently available hardware. All we need is a Gaussian monocycle generator, and a shift register that stores the tap coefficients[2] $\{w[n]\}_{n=0}^{M-1}$. A possible transmitter structure is shown in Fig. 3.

A. Digital Sub-band Hopping

As we discussed in Section III-B, our pulse shaper design can also support multi-band UWB transmissions. Furthermore, our pulse designs are applicable to (fast) frequency hopping (FH) UWB systems. To hop from one frequency band to another, one can simply reset the memory of the shift register, or, use a bank of shift registers and switch among them to select the desired band. Fig. 4 shows such a *digital* Frequency Hopping transmitter structure for UWB communications. The digital architecture implements linear combinations of the baseband Gaussian monocycle, and does not involve analog carriers. This avoids the Carrier Frequency Offset (CFO) effects, which are commonly encountered with analog FH implementations. The limitation of the proposed architecture is the relatively stringent requirement on the clock timing accuracy, which is up to several picoseconds. Also, clock jitter phenomena could impair BER performance in our design.

[2]Because of the symmetry used when applying the Parks-McClellan algorithm, we only need to store half of these tap coefficients in the shift register.

B. Clock Jitter Effects

To implement our designs, the "Timer" block in Figs. 3 and 4 must maintain pico-second accuracy. Time domain corporation has produced application specific integrated circuit (ASIC) timer modules using PulsON technology [17], which can provide the required picosecond accuracy. Thanks to the digital implementation of our design method, even when the timer is imperfect, the tap coefficients can be easily adjusted to satisfy the FCC spectral mask.

Clock jitter in the "Timer" module will affect the BER performance at the receiver. To analyze clock jitter effects, we let $N_f = 1$ in (1) for notational brevity. At the transmitter, the pulse shaper is $p(t) = \sum_{k=0}^{M-1} w[k] g(t - kT_0)$. With clock jitter, the template signal at the receiver will be $v(t) = \tilde{p}(t) - \tilde{p}(t - \Delta)$, with $\tilde{p}(t) = \sum_{k=0}^{M-1} w[k] g(t - kT_0 - \epsilon_k)$, where $\{\epsilon_k\}_{k=0}^{M-1}$ denote the clock jitter errors, which we model as independent uniformly distributed over $[-\beta, \beta]$. Notice that we allow each tap to experience different clock jitter. Over AWGN channels, the decision statistic of the n^{th} transmitted information symbol is $r_n = (\sqrt{\mathcal{E}}/\sqrt{\mathcal{E}_p}) \int p(t - nT_s - s(n)\Delta) v(t - nT_s) dt + \int n(t) v(t - nT_s) dt$; so, the average received SNR γ is calculated to be (assuming $\Delta > T_p$):

$$\gamma = \frac{\mathcal{E}}{N_0} \phi(\beta), \tag{21}$$

$$\phi(\beta) := \text{E}\left\{ \frac{\left[\int p(t)\tilde{p}(t)dt\right]^2}{\int p^2(t)dt \int \tilde{p}^2(t)dt} \right\}, \tag{22}$$

where the expectation is taken over $\{\epsilon_k\}_{k=0}^{M-1}$. Investigating the average error performance in the presence of clock jitter, we have established the following:

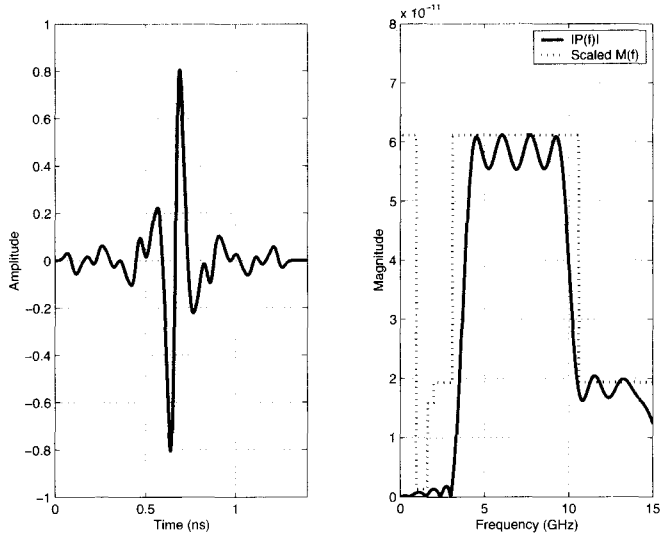

Fig. 5. $L = 16$, optimally designed pulse shaper and its FT with high clock rate $T_0 = 35.7$ps.

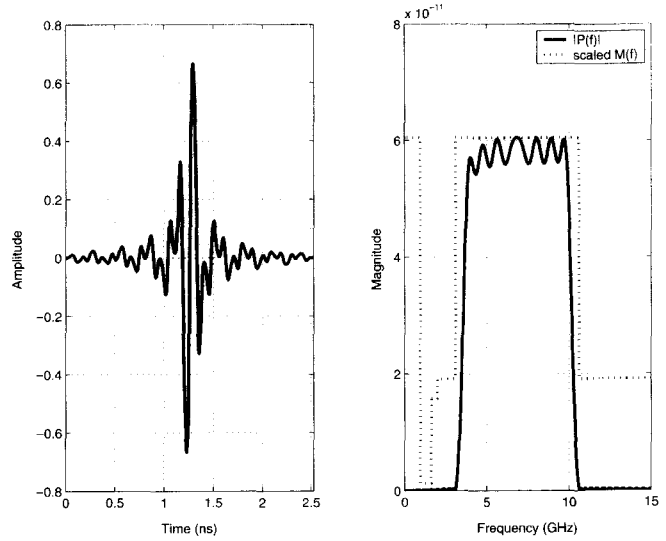

Fig. 6. $L = 16$, optimally designed pulse shaper and its FT with low clock rate $T_0 = 73$ps.

Proposition 2: In a single-user UWB link over AWGN channels, and small clock jitter uniformly distributed over $[-\beta, \beta]$ with $\beta \ll T_g$, the average received SNR γ can be approximated by:

$$\gamma = \frac{\mathcal{E}}{N_0}[1 - \mathcal{C}\beta^2 + O(\beta^3)], \tag{23}$$

where $\mathcal{C}$ is a nonnegative constant given by $\mathcal{C} = -\text{Trace}(\mathbf{A})$, and $\mathbf{A}$ is a matrix defined by (28) in the Appendix.

Proof: See Appendix. □

So long as the clock jitter β remains small, equation (23) shows that it will not lead to major reduction in SNR. Our simulations in Section VII will also confirm the robustness of our designs to clock jitter.

As clock jitter is present in our baseband designs, frequency jitter is present in carrier-modulated systems too. The average received SNR is related to the CFJ f_J as follows [9, Chapter 6]:

$$\gamma = \gamma_0 \text{E}\{\cos^2(2\pi f_J t)\}, \tag{24}$$

where γ_0 is the SNR without CFJ/CFO, and f_J is assumed to be uniformly distributed over $[-\xi_0, \xi_0]$. It follows from (24) that

$$\begin{aligned} \gamma &= \gamma_0 \varphi(\xi_0 t), \\ \varphi(\xi_0 t) &:= \left(\frac{1}{2} + \frac{\sin(4\pi\xi_0 t)}{8\pi\xi_0 t}\right). \end{aligned} \tag{25}$$

From $\varphi(\xi_0 t)$, we deduce that even a small f_J will cause considerable degradation in the average SNR as t increases.

VI. DESIGN EXAMPLES AND COMPARISONS

In this section, we apply the approach of Section III to design pulse shapers for single- and multi-band UWB systems. The Gaussian monocycle parameter f_g is chosen to be 6.85GHz.

A. Single-Band UWB: Clock Rates $T_0 = 35.7$ps *and* 73ps

We choose the sets $\mathcal{F}_1, \mathcal{F}_2, \mathcal{F}_3$ in Section III-A.1 to be $\mathcal{F}_1 = [0, 0.1107]$, $\mathcal{F}_2 = [0.15, 0.33]$, and $\mathcal{F}_3 = [0.3786, 0.5]$. The weight function $\lambda(F)$ is selected to be 2, when $F \in \mathcal{F}_1$ and 1, when $F \in \mathcal{F}_2 \bigcup \mathcal{F}_3$. The reason that we weigh more the band $\mathcal{F}_1$ is because we want the approximation error and thus the energy inside $\mathcal{F}_1$ to be smaller. We only show results for $L = 16$ (digital FIR filter of length $M = 33$). The designed pulse shaper and its FT are plotted in Fig. 5.

Next, we select the sets $\mathcal{F}_1, \mathcal{F}_2$ in Section III-A.2 to be $\mathcal{F}_1 = [0, 0.2263]$ and $\mathcal{F}_2 = [0.28, 0.5]$. The weight $\lambda(F)$ is now 5 in $\mathcal{F}_1$, and 1 in $\mathcal{F}_2$. With $L = 16$, the resulting pulse has duration $T_p = 2.52$ns, and is depicted along with its FT in Fig. 6.

B. Multi-Band UWB: Clock Rate $T_0 = 35.7$ps

Here, we design pulse shapers for $N = 3$ sub-bands. The desired functions, $D_i(f), i = 0, 1, 2$, are as in (16). In the design process, we choose the set $\mathcal{F}$ in (13), as the union of $\mathcal{F}_1 \bigcup \mathcal{F}_2 \bigcup \mathcal{F}_3$, to be $[0, 0.1107] \bigcup [0.1178, 0.1928] \bigcup [0.2, 0.5]$ for the 1^{st} band, $[0, 0.2] \bigcup [0.0.2071, 0.2821] \bigcup [0.2892, 0.5]$ for the 2^{nd} band, and $[0, 0.2892] \bigcup [0.2964, 0.3714] \bigcup [0.3785, 0.5]$ for the 3^{rd} one. The weight function $\lambda(F)$ is chosen to be 5 in $\mathcal{F}_2$, and 1 in $\mathcal{F}_1 \bigcup \mathcal{F}_3$. With $L = 100$, the optimal pulse shapers and their FTs are shown in Fig. 7.

C. Power Efficiency Comparison

As mentioned before, for any pulse shaper $p(t)$, compliance to the FCC mask can be achieved by adjusting the transmit energy per pulse $\mathcal{E}$, or equivalently, the transmit power. We will compare the maximum allowable transmit power limited by the FCC mask corresponding to three pulse shapers: (i) the Gaussian monocycle $g(t)$ with $f_g = 6.85$GHz [c.f. (8)]; (ii) the pulse shaper $p_{16}(t)$ we designed in Section VI-A with time duration 1.3ns (Fig. 5); and (iii) the "prolate-spheroidal" pulse shaper $p_{p-s}(t)$ designed in [7] with the same time duration 1.3ns

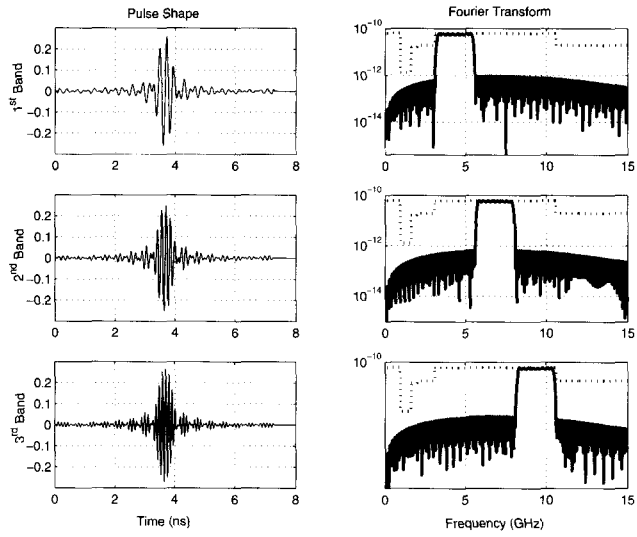

Fig. 7. Optimal multi-band UWB pulse shapers and their FTs, $L = 100$, (3 bands here).

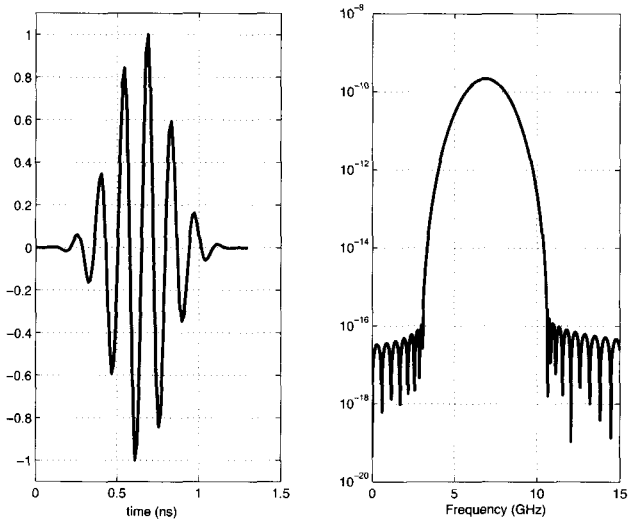

Fig. 8. The "Prolate-Spheroidal" pulse shaper of [7] and its FT.

(Fig. 8).

With $G(f), P_{p-s}(f)$, and $P_{16}(f)$ denoting the FT of $g(t), p_{p-s}(t)$, and $p_{16}(t)$, respectively, their corresponding EIRP spectra are $|G(f)|^2/T_f$, $|P_{p-s}(f)|^2/T_f$, and $|P_{16}(f)|^2/T_f$. Complying to the FCC spectral mask, while transmitting at the maximum allowable power, these pulses need to be scaled so that (see also Fig. 1):

$$\begin{aligned}
\max_f \frac{|\theta_1 G(f)|^2}{T_f} &= -66.3\text{dBm/MHz, (System 2 in Fig.1)} \\
\max_f \frac{|\theta_2 P_{p-s}(f)|^2}{T_f} &= -41.3\text{dBm/MHz,} \\
\max_f \frac{|\theta_3 P_{16}(f)|^2}{T_f} &= -41.3\text{dBm/MHz,}
\end{aligned}$$

where $\theta_1, \theta_2, \theta_3$ are scaling factors. The maximum power corresponding to each pulse shaper is then calculated to be

$$\begin{aligned}
\mathcal{P}_g &= \frac{1}{T_f}|\theta_1|^2 \int |G(f)|^2 df = 0.00387\text{mW}, \\
\mathcal{P}_{p-s} &= \frac{1}{T_f}|\theta_3|^2 \int |P_{p-s}(f)|^2 df = 0.25\text{mW}, \\
\mathcal{P}_{16} &= \frac{1}{T_f}|\theta_2|^2 \int |P_{16}(f)|^2 df = 0.91\text{mW}.
\end{aligned}$$

It is clear that our design utilizes the FCC spectral mask most efficiently.

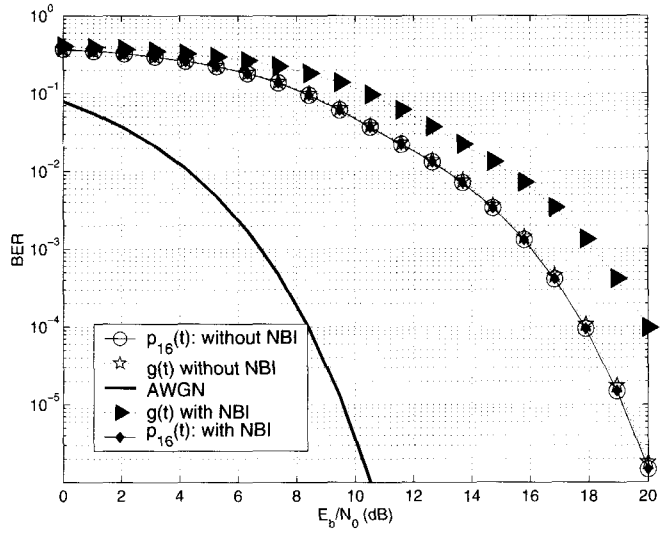

Fig. 9. BER comparison in the presence of NBI.

VII. SIMULATIONS

A. Narrow-Band Interference Avoidance

Since the spectrum from 0.96GHz to 3.1GHz contains the GPS and the 802.11b/g bands, when we designed $p(t)$ to approximate the FT mask $\mathcal{M}(f)$ in Section III, we intentionally minimized the pulse energy over $0.96 - 3.1$GHz to mitigate the interference caused by (and to) these narrow-band systems. Let the PSD of the NBI within this band be $J_0 = 10N_0$, where N_0 is the PSD level of the AWGN. We compare the BER performance of the UWB system in the presence of a multipath channel with two different pulse shapers: the one we designed in Section VI-A with clock rate of 35.7ps, and our basic building block, the popular Gaussian monocycle with $f_g = 6.85$GHz. The multipath channel is generated according to [18], with parameters $(\Lambda, \lambda, \Gamma, \gamma) = (0.0233\text{ns}^{-1}, 2.5\text{ns}^{-1}, 7.1\text{ns}, 4.3\text{ns})$ for an indoor channel with line of sight (LOS) [19]. At the transmitter, the modulated signals are as in (1), with $N_f = 32$, $\Delta = 1.5$ns, $T_c = 4$ns, and $T_f = 100$ns. At the receiver, we used a 16-finger RAKE with spacings ≥ 2ns. Maximum ratio combining (MRC) was employed to combine all fingers' outputs.

In the absence (presence) of NBI, the BER performance of the UWB system with different pulse shapers is plotted in Fig. 9. Clearly, our designed pulse shaper mitigates NBI better than the Gaussian monocycles.

B. Clock Jitter Effects

As shown in Proposition 2, $\phi(\beta)$ is well approximated by $1-\mathcal{C}\beta^2$, when β is small. Here, we will verify this numerically. Utilizing the pulse shaper we designed in Section VI-B for the first band, Fig. 10 depicts the $\phi(\beta)$ generated by simulation. Using the coordinates of the points (β, ϕ) from the simulation, we can fit them to a quadratic function $\phi(\beta) = 1-\mathcal{C}\beta^2$. We plot the result in Fig. 10, which verifies that the receive SNR is robust to small timing jitter values.

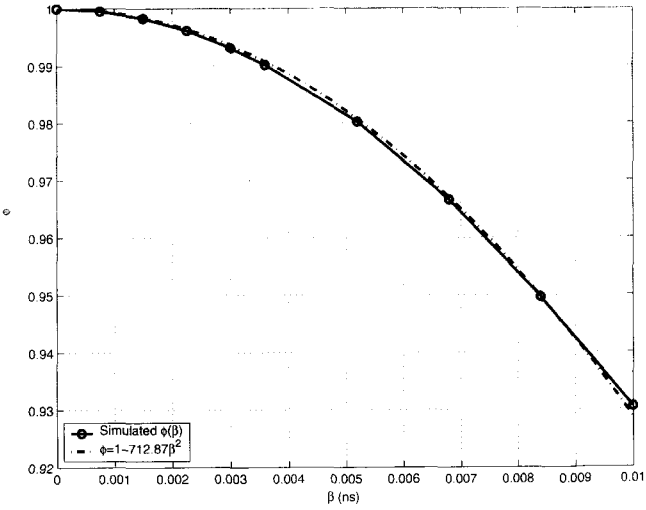

Fig. 10. Timing jitter effects (see (22)).

VIII. CONCLUSIONS

In this paper, we introduced an optimum UWB pulse design methodology, which renders the pulse design problem equivalent to an optimum FIR filter design problem. The resulting pulses not only meet the FCC regulation, but also optimally exploit the allowable bandwidth and power. Utilizing such pulses, baseband UWB transmissions can be designed either as single-band, or as multi-band. Equally important, the novel pulse shapers can support dynamic avoidance of narrow-band interference, as well as implementation of fast frequency hopping, free of analog carriers. We have also shown that the optimal pulse shapers can be implemented without modifying the analog components of existing UWB transceivers.

APPENDIX: PROOF OF PROPOSITION 2

We have $\phi(\beta) = E\{\mathcal{L}\}$, where

$$\mathcal{L}(\epsilon_0, \cdots, \epsilon_{M-1}) = \frac{\left[\int p(t)\tilde{p}(t)dt\right]^2}{\int p^2(t)dt \int \tilde{p}^2(t)dt}. \tag{26}$$

When the clock jitters $\{\epsilon_k\}_{k=0}^{M-1}$ are small, we can expand $\mathcal{L}(\epsilon_0, \cdots, \epsilon_{M-1})$ using Taylor series:

$$\mathcal{L}(\epsilon_0, \cdots, \epsilon_{M-1}) = \mathcal{L}(0, \cdots, 0) + \boldsymbol{\epsilon}^T \nabla\mathcal{L}(0, \cdots, 0) + \frac{1}{2}\boldsymbol{\epsilon}^T \mathbf{A}\boldsymbol{\epsilon} + O(\epsilon^3), \tag{27}$$

where $\boldsymbol{\epsilon} := (\epsilon_0, \cdots, \epsilon_{M-1})^T$, and $\mathbf{A}$ is an $M \times M$ matrix given by:

$$\mathbf{A} := \begin{bmatrix} \frac{\partial^2\mathcal{L}}{\partial\epsilon_0^2} & \frac{\partial^2\mathcal{L}}{\partial\epsilon_0\partial\epsilon_1} & \cdots & \frac{\partial^2\mathcal{L}}{\partial\epsilon_0\partial\epsilon_{M-1}} \\ \frac{\partial^2\mathcal{L}}{\partial\epsilon_1\partial\epsilon_0} & \frac{\partial^2\mathcal{L}}{\partial\epsilon_1^2} & \cdots & \frac{\partial^2\mathcal{L}}{\partial\epsilon_1\partial\epsilon_{M-1}} \\ \vdots & \vdots & \ddots & \vdots \\ \frac{\partial^2\mathcal{L}}{\partial\epsilon_{M-1}\partial\epsilon_0} & \frac{\partial^2\mathcal{L}}{\partial\epsilon_{M-1}\partial\epsilon_1} & \cdots & \frac{\partial^2\mathcal{L}}{\partial\epsilon_{M-1}^2} \end{bmatrix}_{(0,\cdots,0)}. \tag{28}$$

It is easily verified that the gradient of $\mathcal{L}$ at $(0, \cdots, 0)$ is zero; i.e., $\nabla\mathcal{L}(0, \cdots, 0) = \mathbf{0}$. Schwarz's inequality requires $\mathbf{A}$ to be negative semi-definite. Considering that $\{\epsilon_k\}_{k=0}^{M-1}$ are i.i.d. uniformly distributed over $[-\beta, \beta]$, we obtain

$$\begin{aligned} \mathrm{E}\{\mathcal{L}\} &= 1 + \mathrm{Trace}(\mathbf{A})\mathrm{E}\{\epsilon_0^2\} + \mathrm{E}\{\mathrm{O}(\epsilon_0^3)\} \\ &= 1 - \mathcal{C}\beta^2 + O(\beta^3), \end{aligned} \tag{29}$$

where $\mathcal{C} = -\mathrm{Trace}(\mathbf{A})$ is a nonnegative number for $\mathrm{Trace}(\mathbf{A}) \leq \mathbf{0}$, since $\mathbf{A}$ is a negative semi-definite matrix. Equation (29) implies that as long as the clock jitter is much smaller than T_g, the function $\phi(\beta)$ in (22) satisfies $1 - \phi(\beta) \propto \beta^2$, where β is the upper bound of the clock jitter.

REFERENCES

[1] M. Z. Win and R. A. Scholtz, "Impulse radio: How it works," *IEEE Commun. Lett.*, vol. 2, pp. 36–38, Feb. 1998.

[2] FCC Report and Order, *In the Matter of Revision of Part 15 of the Commission's Rules Regarding Ultra-Wideband Transmission Systems*, FCC 02-48, Apr. 2002.

[3] R. A. Scholtz, "Mutiple access with time hopping impulse modulation," in *Proc. Military Communications Conference*, Boston, MA, USA, Oct. 1993, pp. 447–450.

[4] J. D. Choi and W. E. Stark, "Performance of ultra-wideband communications with suboptimal receivers in multipath channels," *IEEE J. Select. Areas Commun.*, vol. 20, no. 9, pp. 1754–1766, Dec. 2002.

[5] P. Withington, "Impulse radio overview," Time Domain Corp., downloadable: *http://user.it.uu.se/~ carle/Notes/UWB.pdf.*

[6] A. V. Oppenheim *et al.*, *Discrete-Time Signal Processing*, 2nd Edition, Prentice Hall, 1999.

[7] B. Parr *et al.*, "A novel ultra-wideband pulse design algorithm," *IEEE Commun. Lett.*, vol. 7, no. 5, pp. 219–221, May 2003.

[8] B. Parr, B. Cho, and Z. Ding, "A new UWB pulse generator for FCC spectral masks," in *Proc. Vehicular Technology Conference*, vol. 3, Apr. 2003, pp. 1664–1666.

[9] J. Proakis, *Digital Communications*, McGraw-Hill, New York, 4th edition, Feb. 2001.

[10] J. Romme and L. Piazzo, "On the power spectral density of time-hopping impulse radio," in *Proc. IEEE Conf. Ulta-Wideband Systems and Technologies*, Baltimore, MD, USA, May 2002, pp. 241–244.

[11] M. Z. Win, "Spectral density of random UWB signals," *IEEE Commun. Lett.*, vol. 6, no. 12, pp. 526–528, Dec. 2002.

[12] J. D. Taylor, *Ultra Wideband Radar Technology*, CRC Press, New York, 2002.

[13] F. Ramirez-Mireles and R. A. Scholtz, "System performance analysis of impulse radio modulation," in *Proc. Radio and Wireless Conference*, Colorado Springs, CO, USA, Aug. 1998, pp. 67–70.

[14] J. Han and C. Nguyen, "A new ultra-wideband, ultra-short monocycle pulse generator with reduced ringing," *IEEE Microwave Wireless Compon. Lett.*, vol. 12, no. 6, pp. 206–208, June 2002.

[15] J. S. Lee, C. Nguyen, and T. Scullion, "New uniplanar subnanosecond monocycle pulse generator and transformer for time-domain microwave applications," *IEEE Trans. Microwave Theory Tech.*, vol. 49, no. 6, pp. 1126–1139, June 2001.

[16] T. W. Parks and J. H. McClellan, "Chebyshev approximation for nonrecur-

sive digital filters with linear phase," *IEEE Trans. Circuit Theory*, vol. CT-19, no. 2, pp. 189–194, Mar. 1972.

[17] D. Kelly *et al.*, "PulsON second generation timing chip: Enabling UWB througn precise timing," in *Proc. IEEE Conf. Ultra-Wideband Systems and Technologies*, Baltimore, MD, USA, May 2002, pp. 117–121.

[18] A. A. M. Saleh and R. A. Valenzuela, "A statistical model for indoor multipath propagation," *IEEE J. Select. Areas Commun.*, vol. 5, no. 2, pp. 128–137, Feb. 1987.

[19] IEEE P802.15 Working Group for WPAN, *Channel Modeling Sub-Committee Report Final*, IEEE P802.15-02/368r5-SG3a, Nov. 2002.

Xiliang Luo received his B.S. degree in Physics from the Peking University, Beijing, China, in 2001, and M.Sc. degree in Electrical Engineering from the University of Minnesota, in 2003. He is currently a Ph.D. student in the Department of Electrical and Computer Engineering at the University of Minnesota. His research interests lie in signal processing and communication. Currently, he is focusing on topics in Ultra-Wideband communications.

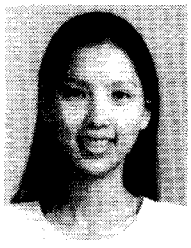

Liuqing Yang received her B.S. degree in Electrical Engineering from the Huazhong University of Science and Technology, Wuhan, China, in 1994, and M.Sc. degree in Electrical Engineering from the University of Minnesota, in 2002. She is currently a Ph.D. candidate in the Department of Electrical and Computer Engineering, at the University of Minnesota. Her research interests include communications, signal processing, and networking. Currently, she has a particular interest in Ultra Wideband (UWB) communications. Her research encompasses synchronization, channel estimation, equalization, multiple access, space-time coding, and multicarrier systems.

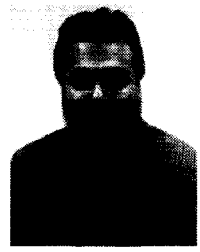

Georgios B. Giannakis received his Diploma in Electrical Engineering from the National Technical University of Athens, Greece, 1981. From September 1982 to July 1986 he was with the University of Southern California (USC), where he received his MSc. in Electrical Engineering, 1983, MSc. in Mathematics, 1986, and Ph.D. in Electrical Engineering, 1986. After lecturing for one year at USC, he joined the University of Virginia in 1987, where he became a professor of Electrical Engineering in 1997. Since 1999 he has been a professor with the Department of Electrical and Computer Engineering at the University of Minnesota, where he now holds an ADC Chair in Wireless Telecommunications. His general interests span the areas of communications and signal processing, estimation and detection theory, time-series analysis, and system identification – subjects on which he has published more than 175 journal papers, 325 conference papers, and two edited books. Current research focuses on transmitter and receiver diversity techniques for single- and multi-user fading communication channels, complex-field and space-time coding, multicarrier, ultra-wide band wireless communication systems, cross-layer designs, and distributed sensor networks. G. B. Giannakis is the (co-) recipient of four best paper awards from the IEEE Signal Processing (SP) Society (1992, 1998, 2000, 2001). He also received the Society's Technical Achievement Award in 2000. He served as Editor in Chief for the *IEEE SP Letters*, as Associate Editor for the *IEEE Trans. on Signal Proc.* and the *IEEE SP Letters*, as secretary of the SP Conference Board, as member of the SP Publications Board, as member and vice-chair of the Statistical Signal and Array Processing Technical Committee, as chair of the SP for Communications Technical Committee, and as a member of the IEEE Fellows Election Committee. He is currently a member of the IEEE-SP Society's Board of Governors, the Editorial Board for the *Proceedings of the IEEE*, and chairs the steering committee of the *IEEE Trans. on Wireless Communications*.